ACS OMEGA

http://pubs.acs.org/journal/acsodf

Article

Self-Therapeutic Cobalt Hydroxide Nanosheets ($Co(OH)_2$ NS) for Ovarian Cancer Therapy

Muhammad Adeel, Salvatore Parisi, Matteo Mauceri, Kanwal Asif, Michele Bartoletti, Fabio Puglisi, Isabella Caligiuri, Md. Mahbubur Rahman, Vincenzo Canzonieri, and Flavio Rizzolio*

Cite This: *ACS Omega* 2021, 6, 28611−28619

Read Online

ACCESS | Metrics & More | Article Recommendations | Supporting Information

ABSTRACT: High-grade serous ovarian cancer (HGSOC) is one of the major life-threatening cancers in women, with a survival rate of less than 50%. So far, chemotherapy is the main therapeutic tool to cure this lethal disease; however, in many cases, it fails to cure HGSOC even with severe side effects. Self-therapeutic nanomaterials could be an effective alternative to chemotherapy, facilitated by their diverse physicochemical properties and the ability to generate reactive species for killing cancer cells. Herein, inorganic cobalt hydroxide nanosheets ($Co(OH)_2$ NS) were synthesized by a simple solution process at room temperature, and morphological, spectroscopic, and crystallographic analyses revealed the formation of $Co(OH)_2$ NS with good crystallinity and purity. The as-prepared $Co(OH)_2$ NS showed excellent potency, comparable to the FDA-approved cisplatin drug to kill ovarian cancer cells. Flow cytometric analysis (nnexin V) revealed increased cellular apoptosis for $Co(OH)_2$ NS than cobalt acetate (the precursor). Tracking experiments demonstrated that $Co(OH)_2$ NS are internalized through the lysosome pathway, although relocalization in the cytoplasm has been observed. Hence, $Co(OH)_2$ NS could be an effective self-therapeutic drug and open up an area for the optimization of self-therapeutic properties of cobalt nanomaterials for cancer treatment.

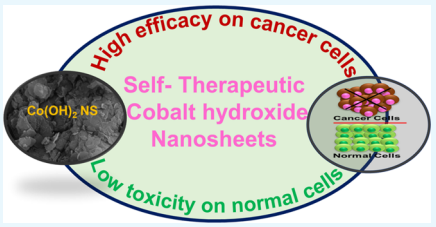

INTRODUCTION

High-grade serous ovarian cancer (HGSOC) represents about 70% of all ovarian cancers and is characterized by high lethality.[1] The main therapeutic approach of HGSOC includes surgery and chemotherapy.[2,3] Chemotherapy based on platinum salts is considered essential for HGSOC treatment[4] but has many side effects like other systemic therapies,[5−8] and resistance to chemotherapy appears almost in all of the patients with recurrent disease, limiting the effectiveness of treatments.[2] Other drugs with clinical benefits approved by FDA are paclitaxel, doxorubicin, capecitabine, topotecan, and PARP inhibitors, and many others are under clinical trials, but still, these treatments are not resolutive.[4,8,9]

A way to improve efficacy and decrease toxicity is the development of delivery systems using different nanomaterials taking advantage of their different intrinsic properties.[10,11] Nanosized materials (e.g., nanoparticles) (NMs) are currently becoming a topic of interest in drug delivery applications for cancer therapy[12−14] since they are not expensive, easy to synthesize, and could be functionalized to be selective for and internalized by tumor cells.[15,16] Differently from the solubility problems of drugs (many therapeutic drugs fail in clinical trials due to solubility issues),[17] nanoparticles could be solubilized in water due to their nanometer size and acquire excellent pharmacokinetic parameters due to their versatility in physiochemical properties.[18,19] NMs have a tunable size and could be designed to efficiently take advantage of the enhanced permeability and retention (EPR) effects of some tumors and actively internalize by the membrane of cancer cells or to escape the scavenger macrophages before reaching to the tumor microenvironment.[20] Several NMs have been utilized in ovarian cancer therapy like liposomes, micelles, dendrimers, hydrogels, and many other organic and inorganic compounds.[8,21−23] Although a large number of NMs have been developed as delivery systems, so far only up to 1% of the drug reaches the tumoral sites and hence making this approach far from real applications.[24,25]

These expectations could be fulfilled through nanomaterials using their self-therapeutic (intrinsic therapeutic properties, without loaded drugs) properties.[24] Recently, the self-therapeutic trend of nanomaterials has been increasing continuously because of their versatile intrinsic properties, cost reduction, and ease of use in therapeutic applications.[24,26] Inorganic materials have elicited considerable attraction in this regard because of their intrinsic antitumor abilities, and many (like SiO2, Ag, Au, MOFs, composites, etc.) have been used even if they are often not effective in killing aggressive tumor cells.[24] In humans, cobalt is a trace element necessary for the biological activity of vitamin B12 and at a daily assumption

Received: June 8, 2021
Accepted: August 23, 2021
Published: October 19, 2021

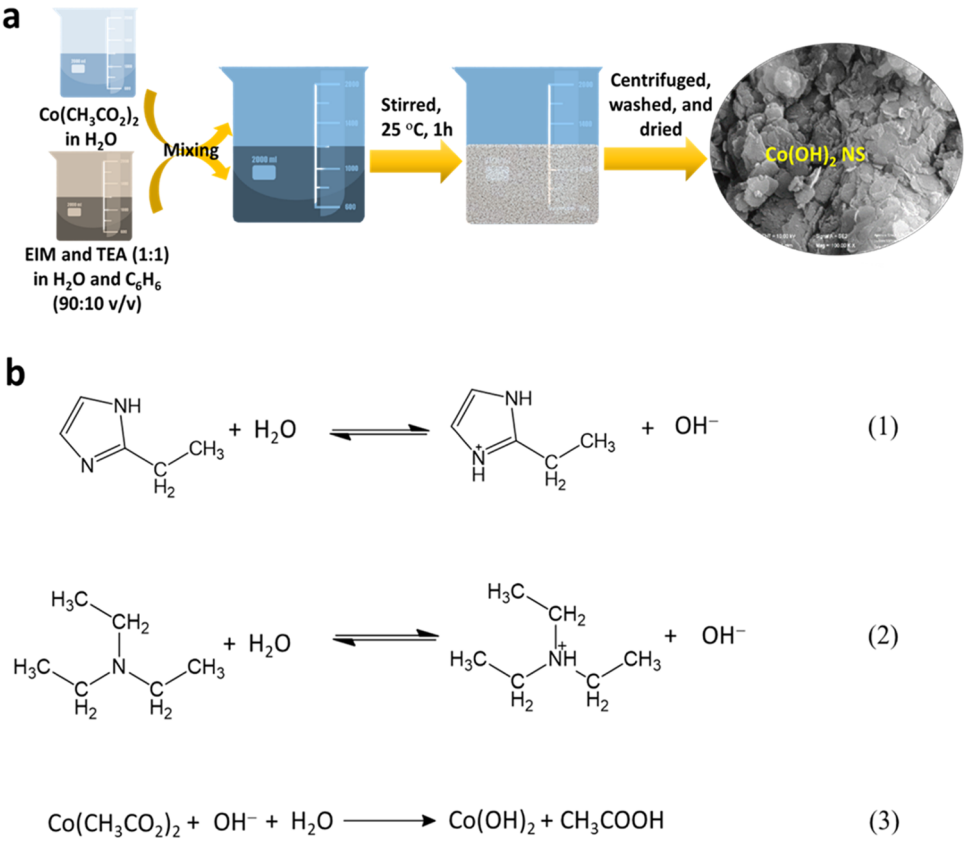

Figure 1. (a) Schematic illustration of the synthesis of $Co(OH)_2$. (b) Plausible reaction mechanisms for the formation of $Co(OH)_2$.

above 1 mg could create adverse reactions including hematological and thyroid problems.[27] Starting from the 1950s, cobalt has been available on the market to treat children and adult anemia (now discontinued),[28] and many research groups have introduced cobalt-based therapeutic systems for different cancer therapies and in vivo imaging purposes.[29] Thamilarasan et al. utilized cobalt(III) complexes as a potential anticancer agent, demonstrating the ability of interacting with DNA.[30] Klein et al. prepared magnetite and cobalt ferrite nanoparticles with better biocompatibility and water dispersibility as an enhancer of reactive oxygen species (ROS) formation for radiation therapy.[31] Bejarbaneh et al. synthesized cobalt hydroxide nano-flasks functionalized with glutamic acid and conjugated with thiosemicarbazide as an anticancer agent against human breast cancer cells.[32] In another report, it was described that cobalt complexes were effective in overcoming multidrug resistance and as an alternative to cisplatin in vivo.[33] Heffern et al. and Munteanu et al. separately reviewed the cobalt-based complexes for therapeutic, imaging, and drug delivery applications.[29,34] However, no studies have been reported for the treatment of ovarian cancer with inorganic cobalt or its derivatives.

Here, in this study, we propose for the first time two-dimensional (2D) cobalt hydroxide nanosheets ($Co(OH)_2$ NS) for HGSOC treatment. Very simple and cost-effective solutions have been utilized to synthesize $Co(OH)_2$ NS at room temperature (RT). $Co(OH)_2$ NS were investigated through different characterization techniques and tested as an effective drug for ovarian cancer cells. Different experiments were performed to check the toxic effects, localization, and internalization of $Co(OH)_2$ NS.

RESULTS AND DISCUSSION

Synthesis of $Co(OH)_2$ NS. A water−benzene mixed solvent system was employed to prepare $Co(OH)_2$ NS, and the synthesis procedure is schematically shown in Figure 1a. Figure 1b shows the possible reaction pathways for the formation of $Co(OH)_2$ NS. Initially, basic 2-ethylimidazole (EIM) and trimethylamine (TEA) could react with water-forming hydroxyl (OH) ions (eqs 1 and 2).[36] Subsequently, the OH in the solution react with Co^{2+} of $Co(CH_3CO_2)_2$ and form $Co(OH)_2$ (eq 3). Upon stirring, the water immiscibility and low specific gravity of benzene can result in an outward pushing force and facilitate the formation of NS.

Morphological Characterizations. Figure 2a,b shows the field emission scanning electron microscopy (FE-SEM) images of the as-synthesized $Co(OH)_2$, which revealed the formation of interconnected 2D NS with a variable size range (ca. 10−120 nm). The low transparency to the electron beam in the high-resolution transmission electron microscope (HR-TEM) image (Figure 2c) further suggests the formation of interconnected 2D NS, which is consistent with the FE-SEM results. The bright spots with a ringlike pattern having *d*-spacings of ca. 2.4, 1.45, 1.26, and 0.99 Å with the corresponding *hkl* reflections of (001), (100), (011), and $(10\bar{2})$ obtained from the selected area diffraction pattern (SAED) (Figure 2d), suggested the good crystallinity and purity of $Co(OH)_2$.[3737] The (001) plane having a lattice spacing of ca. 2.40 Å between the adjacent fringes of $Co(OH)_2$NS crystals (Figure 2e,f) was close to the measured *d*-spacing value from the SAED result.[37] All of the structural analyses confirmed the high crystallinity and purity of the as-synthesized $Co(OH)_2$NS.

https://doi.org/10.1021/acsomega.1c03010
ACS Omega 2021, 6, 28611−28619

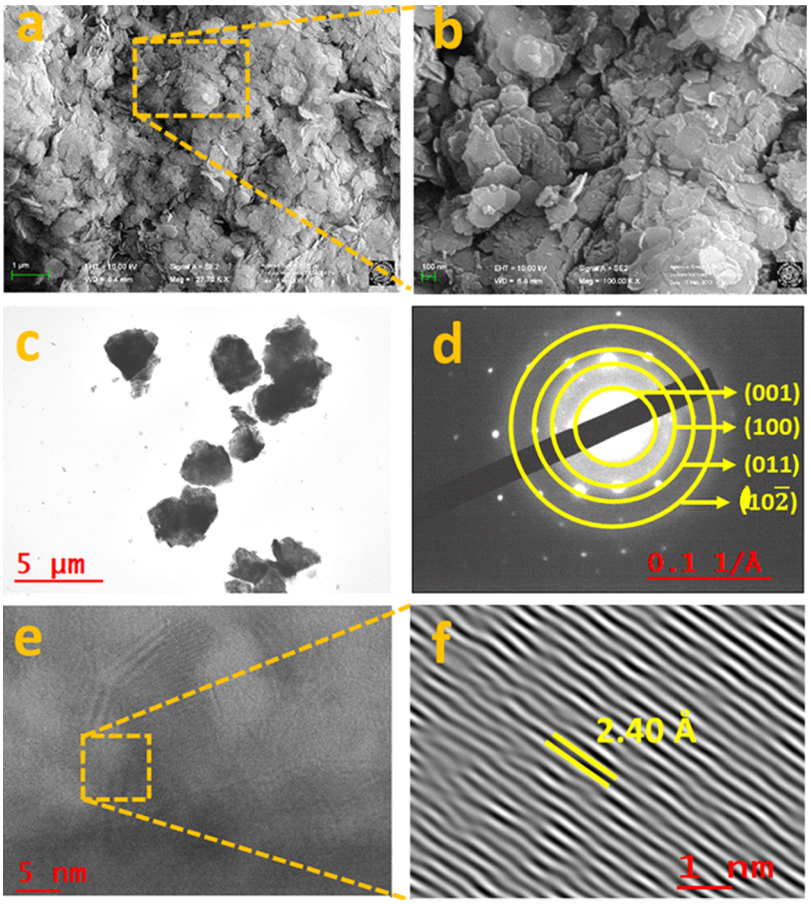

Figure 2. (a, b) FE-SEM images, (c) TEM, and (d) SAED pattern of the as-synthesized $Co(OH)_2$ NS. (e) HR-TEM images and (f) magnified calibrated lattice fringes of $Co(OH)_2$ NS for the (001) plane.

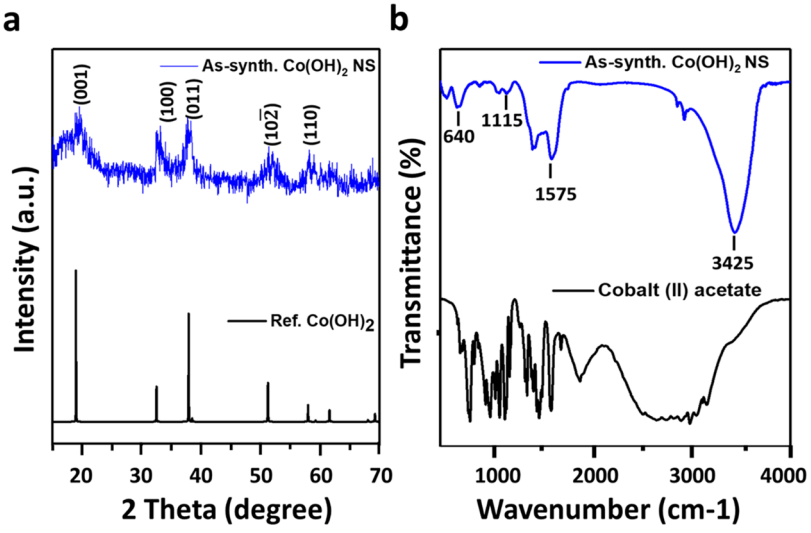

Figure 3. (a) XRD powder patterns of the as-synthesized $Co(OH)_2$ NS together with the simulated pattern of $Co(OH)_2$. (b) FTIR spectrum of cobalt acetate and as-prepared $Co(OH)_2$ NS.

Structural Characterizations. Figure 3a shows the XRD powder pattern of the as-prepared $Co(OH)_2$NS along with the simulated XRD pattern of $Co(OH)_2$. The simulated pattern was perfectly matched with the XRD pattern of $Co(OH)_2$NS without the presence of impurity peaks. The intense and sharp XRD peaks indicated the high crystallinity of $Co(OH)_2$ NS, consistent with the TEM analyses. The major peaks of $Co(OH)_2$NS at 2θ angles of ca. 19.30, 32.60, 38.10, 51.35, 57.98, and 61.75° could be ascribed to the *hkl* reflections of (001), (100), (011), (10$\bar{2}$), and (110), respectively.[38] A Fourier transform infrared spectroscopy (FTIR) study was performed to investigate the chemical bonding in $Co(OH)_2$ NS (Figure 3b), which showed a strong absorption peak of O−H stretching at ca. 3425 cm^{-1}, arising from the Co−OH

https://doi.org/10.1021/acsomega.1c03010
ACS Omega 2021, 6, 28611−28619

groups and the adsorbed water molecules.[39] The absorption bands that appeared at ca. 1115 and 1575 cm^{-1} could be ascribed to C−O stretching and C−H bending, respectively. These bands could be originated from the adsorbed or intercalated CH_3COO^- ions into the $Co(OH)_2$ NS.[40] The low-intense FTIR absorption band observed at ca. 640 cm^{-1} could be assigned to both Co−OH and Co−O bending vibrations, as similarly observed for $Co(OH)_2$, $Ni(OH)_2$, and $Ni(OH)_2$−$Co(OH)_2$ layered double hydroxide.[38,39] The stability of $Co(OH)_2$ NS was examined by creating artificial in vivo body-like conditions in two different pHs (7.4 and 5.5) at 37 °C. The samples were collected at different time intervals after the treatment and analyzed by UV−vis absorption measurements (Figure S1). Results demonstrated the appearance of $Co(OH)_2$ absorption band at about 230 nm without any noticeable shifting in the absorbance maxima at both pHs for up to 1 week, suggesting the high stability of $Co(OH)_2$ NS as a self-therapeutic nanomedicine.

Cell Viability. Cell viability measurements were performed on different cell lines (ovarian and colon cancer cell lines and normal cells). The results are summarized in Table 1. For the

Table 1. IC_{50} Values of $Co(OH)_2$ NS, Cobalt Acetate, and Cisplatin[a]

	drug	AV	SD	ratio
A2780	cisplatin	0.05	0.01	1
	$Co(OH)_2$ NS	1.6	0.2	32
	cobalt acetate	5.5	2.6	110
OVCAR-3	cisplatin	0.6	0.1	1
	$Co(OH)_2$ NS	11.4	2.2	19
	cobalt acetate	12.1	1.7	20
HCT-116	cisplatin	3.1	0.3	1
	$Co(OH)_2$ NS	6.7	0.4	2
	cobalt acetate	41.6	1.6	13
NIH-3T3	cisplatin	13.1	5.5	1
	$Co(OH)_2$ NS	69	13	5
	cobalt acetate	82.4	3.8	6
MRC-5	cisplatin	0.4	0.1	1
	$Co(OH)_2$ NS	31.9	3.6	80
	cobalt acetate	29.8	11.4	75

[a]Values are expressed as μg/mL.

IC_{50} values of $Co(OH)_2$ NS are in the range of 1.6−11.4 μg/mL, compared to those of the cobalt acetate precursor (5.5−41.6 μg/mL). These results suggest that inside the cells, $Co(OH)_2$ NS could release Co^{2+} ions and exert its toxic activity.[41] Compared with cisplatin, in cancer cells, $Co(OH)_2$ NS is less potent in the range of 2- to 32-fold. Conversely, in human MRC-5 fibroblast cells, the toxicity of $Co(OH)_2$ NS is 80-fold less. The calculate ratio of potency/toxicity of $Co(OH)_2$ NS vs cisplatin is 2.5- to 40-fold higher. In mouse NIH-3T3 fibroblast cell line, the $Co(OH)_2$ NS is still less toxic than cisplatin (5-fold less). The results suggest that $Co(OH)_2$ NS could be a possible future candidate as an alternative drug effective for late-stage tumors. The versatility of the proposed $Co(OH)_2$ NS for other cancers was tested on the HCT-116 colon cancer cell line and showed promising potency and comparable results with FDA-approved compounds.

Evaluation of Cell Death. Apoptosis (Annexin V) was evaluated using flow cytometric analysis with $Co(OH)_2$NS (50 μg/mL), cobalt acetate (50 μg/mL), and cisplatin (6 μg/mL; 20 μM) as the reference drug at different time points. All of the results are summarized in Figure 4. No apoptosis has been seen in the untreated set of experiments, while cisplatin, cobalt acetate, and $Co(OH)_2$ NS promptly induced apoptosis after 6 h. Both early apoptosis and late apoptosis were observed starting from 6 h and increased with time. The apoptosis is much higher in $Co(OH)_2$ NS-treated cells compared to cobalt acetate-treated cells at any time point. These results confirmed that $Co(OH)_2$NS could be an alternative candidate that could cause earlier apoptosis and cell death in aggressive tumors.

Intracellular Localization. Lysosomes have long been known to play a key role in the degradation of extracellular materials, including chemotherapeutics agents.[42] The colocalization experiments were performed to evaluate the amount of $Co(OH)_2$ NS trafficking to lysosomes. The experiments were performed in the A2780 ovarian cancer cell line (Figure 5). The nucleus was labeled with Hoechst 33342 (blue), lysosome with LysoTracker Green DND-26 (green), and $Co(OH)_2$ NS was labeled with rhodamine B (red). $Co(OH)_2$ NS were analyzed with a fluorescence microscope after 1, 6, and 24 h. It was observed that $Co(OH)_2$ NS were uptaken at each time point. It was demonstrated that $Co(OH)_2$ NS started internalizing even after 1 h. The colocalization of $Co(OH)_2$ NS and lysosomes was evaluated with Pearson's correlation coefficient (R) after 24 h. The "R" value was found to be 0.43 for $Co(OH)_2$ NS, meaning that $Co(OH)_2$ NS partially localized to the lysosomes and could relocalize to the cytoplasm avoiding degradation.

$Co(OH)_2$ NS Are Effective in Killing Cancer Organoids from High-Grade Ovarian Cancer Patients. More than 30% of patients at the late stage of ovarian cancer will develop ascites. Ascites are treated indirectly with chemotherapy, and paracentesis is used to alleviate the symptoms.[43] Ascites contain free-floating cells that are responsible for intraperitoneal metastasis.[44]

To test the effectiveness of $Co(OH)_2$ NS, cancer organoids were generated. Cancer organoids are the last frontiers for ex vivo testing of drugs[45−48] that replicate the response of patients in clinic.[49] Two HGSOC-derived organoids from ascites (Pat A, B) and one high-grade endometroid ovarian cancer from a primary tumor (Pat C) were treated with cobalt acetate and $Co(OH)_2$ NS. Immunohistochemistry (IHC) analysis showed the expression of typical markers of HGSOC, CA125 (cancer antigen 125), WT-1 (Wilms tumor 1), and Pax8 (Paired box 8) (Figure S2). $Co(OH)_2$ NS are effective in the range of 7−26 μg/mL. The potency of $Co(OH)_2$ NS is similar for ascites and primary tumors, suggesting a possible application of them in chemotherapy-naive and heavily treated patients who are resistant to most of the drugs (Table 2).

Compared to cobalt acetate, $Co(OH)_2$ NS are more effective (p value < 0.05) (Figure S3). The median values for $Co(OH)_2$ NS and cobalt acetate are 11 and 29, respectively.

DISCUSSION

Cobalt is available to humans through vitamin B12 or cyanocobalamin, an essential vitamin for many physiological processes that include DNA and aminoacidic synthesis among others. The active forms of vitamin B12, methylcobalamin and adenosylcobalamin, are the cofactors of essential enzymes methionine synthase (MS) and methylmalonyl-CoA mutase (MCM), respectively.[50] Deficiency of vitamin B12 is responsible for or associated with many diseases, including megaloblastic anemia, methylmalonic aciduria, hyperhomocys-

https://doi.org/10.1021/acsomega.1c03010
ACS Omega 2021, 6, 28611−28619

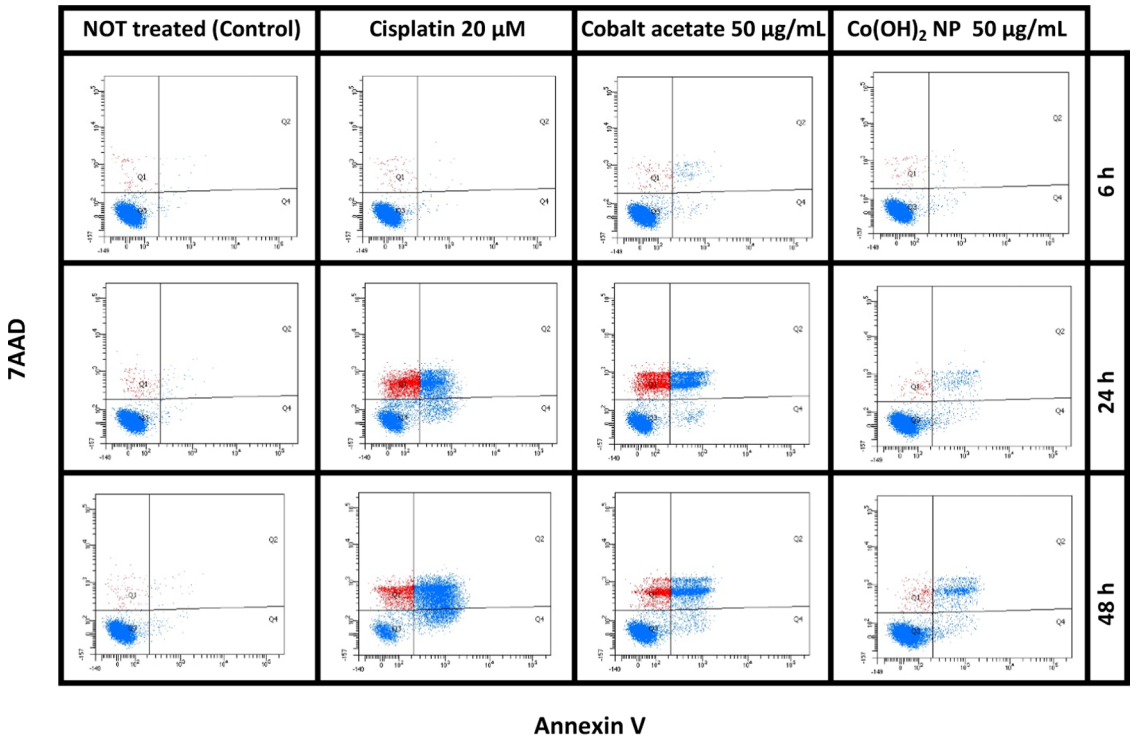

Time (hours)	Sample name	Late Apoptosis % (Q2)		Early Apoptosis % (Q4)	
		Average	SD	Average	SD
6	Not treated	0.05	0.02	0.08	0.04
	Cisplatin 20 μM	0.05	0.01	0.10	0.02
	Cobalt acetate 50 μg/mL	0.13	0.02	0.18	0.01
	$Co(OH)_2$ NP 50 μg/mL	0.46	0.06	0.23	0.02
24	Not treated	0.14	0.04	0.14	0.03
	Cisplatin 20 μM	8.66	0.05	2.40	0.04
	Cobalt acetate 50 μg/mL	1.18	0.04	0.58	0.04
	$Co(OH)_2$ NP 50 μg/mL	8.97	0.33	0.79	0.01
48	Not treated	0.08	0.02	0.17	0.02
	Cisplatin 20 μM	18.08	1.24	5.29	0.20
	Cobalt acetate 50 μg/mL	3.36	0.04	0.89	0.04
	$Co(OH)_2$ NP 50 μg/mL	9.26	1.23	1.13	0.04

Figure 4. Top: An example of apoptosis analysis of cobalt acetate, $Co(OH)_2$ NS, and cisplatin at different time points. Q1, dead cells; Q2, late apoptosis; Q3, healthy cells; Q4, early apoptosis. Bottom: Values (μg/mL) of early apoptosis and late apoptosis from three experiments.

teinemia, and cobalamin neuropathy.[51] Treatment of anemia with a range of 25−150 mg of $CoCl_2$/day has been utilized for many years, but adverse effects drive clinicians to alternative therapies.[52,53,41] Excess of cobalt in the blood has been linked to hematological (range: 0.2−1 mg Co/kg per day), thyroid (range: 0.5−2.7 mg Co/kg per day), neurological (0.3 mg Co/kg per day), and cardiac (range: 0.04−0.07 mg Co/kg per day) effects.[41] As observed, free cobalt ions are responsible for the manifested toxicity.[51] Cobalt ions could generate ROS (Fenton-like reaction) and interfere with the activity of proteins and ions necessary for cellular and organ physiology, such as calcium, iron, iodine, mitochondrial functions, and erythropoiesis.[41]

Starting from these concepts, cobalt complexes that are sufficiently stable during blood circulation will avoid systemic toxicity, in turn releasing cobalt ions after the accumulation in tumors due to the EPR effects and acidic pH typical of the tumor microenvironment. Inside the tumors, the release of cobalt ions could exert their toxic activity. In this research, we developed highly stable cobalt hydroxide nanosheets by a novel solution synthetic process root with an optimal potency/toxicity ratio. The as-synthesized nanosheets were characterized using different techniques to confirm the morphology and crystal structures and showed a sheetlike structure that was confirmed by SEM and TEM analyses. Furthermore, the purity of the cobalt hydroxide nanosheets was examined for their crystal structure using X-ray and FTIR spectroscopies. The X-ray results having distinct crystal planes of cobalt hydroxide agree with the SAED of TEM results with concentric bright rings. The as-synthesized nanosheets were used on different cancer cell lines. The results showed that the cytotoxicity of the cobalt acetate (the precursor) and $Co(OH)_2$ NS showed toxic activity in the same range for cancer cells. Compared to cisplatin, $Co(OH)_2$ NS is less toxic with a favorable potency/toxicity ratio. Flow cytometric analysis (Annexin V) was performed to check cellular apoptosis, and results showed an

https://doi.org/10.1021/acsomega.1c03010
ACS Omega 2021, 6, 28611−28619

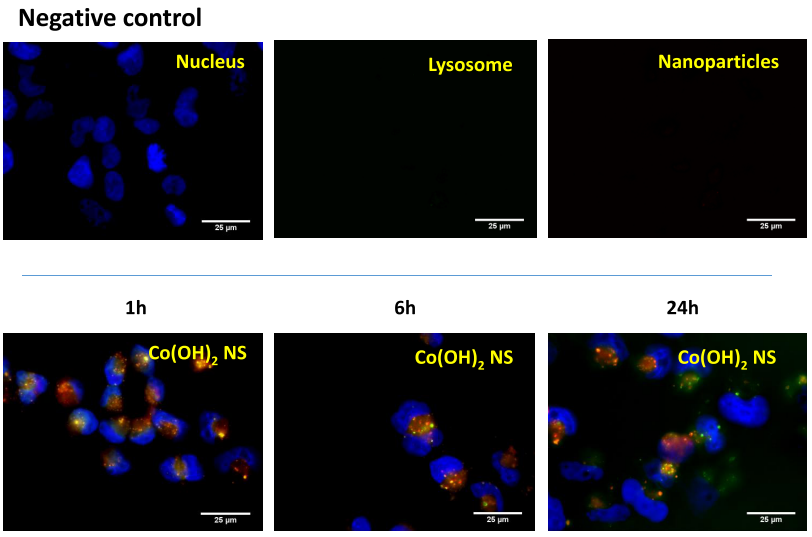

Figure 5. LysoTracker analysis of $Co(OH)_2$ NS for cell internalization study. Fluorescence microscopy images of rhodamine-labeled $C_O(OH)_2$ NS in A2780 ovarian cancer cells after 1, 6, and 24 h, from the left to the right, respectively. Negative control (only nuclei staining, top) was used to set up fluorescence intensity and avoid background signal. The panels in each row show fluorescence from Hoescht 33342 (nuclei stained blue), LysoTracker Green (lysosome stained green), and rhodamine B ($C_O(OH)_2$ NS stained red) and merged images. In merged images, the colocalization of rhodamine with LysoTracker Green appears as yellow areas.

Table 2. IC_{50} Values (μg/mL) of Cobalt Acetate and $Co(OH)_2$ NS in Cancer Organoids Derived from Two HGSOC Ascites Patients (Pat A, B) and One High-Grade Endometroid Tumor Patient (Pat C)[a]

patients	derived from	cobalt acetate	$Co(OH)_2$ NS	doxorubicin
A	ascites	28 ± 4	7 ± 3	1.8 ± 0.4
B	ascites	41 ± 13	26 ± 27	0.09 ± 0.03
C	primary tumor	22 ± 12	16 ± 5	0.9 ± 0.3

[a]Data were obtained from five replicates. The numbers represent mean and standard deviation.

increase in apoptosis that was much more evident for $Co(OH)_2$ NS than cobalt acetate. Colocalization and cellular internalization of $Co(OH)_2$ NS were performed using a LysoTracker marker. The results indicated an active internalization of $Co(OH)_2$ NS that can escape the lysosomal degradation pathway.

All of these results showed that $Co(OH)_2$ NS are promising to inhibit the growth of aggressive cancer cells and could be a potential candidate to cure many other late-stage tumors. However, further in vivo studies are required to evaluate the pharmacokinetic parameters and the toxic effects on healthy organs.

CONCLUSIONS

In summary, $Co(OH)_2$ NS synthesized by a simple solution process are used as a self-therapeutic drug for treating HGSOC. The results revealed that the cytotoxicity of the cobalt acetate (the precursor) and the as-synthesized high-purity and crystalline $Co(OH)_2$ NS showed toxic activity in the same range for cancer cells. Compared to cisplatin, $Co(OH)_2$ NS are less toxic with a favorable potency/toxicity ratio. Flow cytometric analysis (Annexin V) showed an increase in cellular apoptosis that was much more evident for $Co(OH)_2$ NS than cobalt acetate. Furthermore, colocalization and cellular internalization experiments of $Co(OH)_2$NS using a LysoTracker marker indicated an active internalization of $Co(OH)_2$ NS that can escape the lysosomal degradation pathway. Although a high concentration of cobalt is toxic for humans, nanoformulations have been demonstrated to be potentially safe at least at the preclinical level. Thus, this study opens up a window to develop cobalt-based nanomaterials as a self-therapeutic nanomedicine for cancer therapy.

MATERIALS AND METHODS

Materials and Reagents. Cobalt(II) acetate ($Co(CH_3CO_2)_2$), (99.99%), trimethylamine (TEA) (99%), 2-ethylimidazole (EIM) (98%), benzene (99.8%), and absolute ethyl alcohol were purchased from Sigma-Aldrich (St. Louis, MO). A Millipore Milli-Q Biocell A10 water purifying system was used to prepare ultrapure water. A2780 (Sigma-Aldrich, St. Louis, MO), OVCAR-3, HCT-116, and MRC-5 (ATCC, Manassas, VA) cell lines were grown accordingly to the manufacturers' instructions. LysoTracker Green DND-26, Hoechst 33342, and rhodamine B were purchased from Thermo Fisher Scientific (Waltham, Massachusetts).

Synthesis of $Co(OH)_2$ NS. A simple solution process was utilized to prepare pure $Co(OH)_2$ NS. In brief, a solution of $Co(CH_3CO_2)_2$ (0.3 g) was prepared in a beaker using ultrapure water (50 mL). In another beaker, a mixed solution of EIM (0.40 g) and TEA (0.40 g) was prepared using 50 mL of a mixed solvent of water and benzene (90:10, v/v). Then, both solutions were mixed and stirred vigorously at room temperature (RT) for 1 h. After completing the reaction, the precipitate was collected by the centrifuge method at 6000 RPM, washed with water and ethanol, and dried in a vacuum oven at 100 °C for 2 h. The as-synthesized $Co(OH)_2$ NS were stored in an airtight vial for further characterization and application purposes.

Apparatus and Measurements. A field emission scanning electron microscope (FE-SEM, Carl Zeiss Sigma VP, Germany) and a high-resolution transmission electron microscope (HR-TEM, JEM-2100 (HRP)) were utilized to analyze the morphology of the synthesized $Co(OH)_2$ NS. HR-TEM was used to characterize the selected area diffraction pattern (SAED) and the lattice fringe of the $Co(OH)_2$ NS. An

https://doi.org/10.1021/acsomega.1c03010
ACS Omega 2021, 6, 28611−28619

X-ray diffractometer (XRD, Philips) with a Cu Kα radiation (λ = 1.5406 Å) and a Fourier transform infrared (FTIR) spectrophotometer (MIDAC, M4000) were used to characterize the structural properties of $Co(OH)_2$ NS. To calculate IC_{50} values, luminescence was read with a Tecan infinite M1000 Pro instrument (Tecan, Männedorf, Switzerland). Annexin V was evaluated with a BD FACSCantoII instrument (BD Biosciences, San Jose, CA). Fluorescence images were capture with a Nikon Ti Eclipse inverted microscope (Nikon, Minato City, Tokyo, Japan).

Cell Viability. $Co(OH)_2$ NS were tested on different cell lines that were seeded in 96-multiwell plates at a density of 1×10^3 (cancer cells) or 8×10^3 (MRC-5 cells). Cell viability was measured using the CellTiter-Glo assay system according to the manufacturer's instructions[4] (Promega, Madison, Wisconsin) after 96 h. Six serial dilutions 1:10 of the compounds were utilized to calculate the IC_{50} values with GraphPad software utilizing the nonlinear regression method.

Organoids were plated as single cells as possible (around 1000 cells) in five replicates and treated with six serial dilutions 1:10 of the compounds and analyzed after 96 h as cell lines.

Stability of $Co(OH)_2$ NS. An artificial in vivo system has been developed by mixing Co(OH)2 NS (3 mg/mL) in physiological solutions having two different pH values (pH 5.5 and pH 7.4). Then, the solutions were placed in an incubator at 37 °C. The samples were collected at different-day intervals (0−7; DO, D1, D2, D3, D5, and D7), centrifuged, and collected. Then, the UV−vis absorption spectra of the samples were measured by dispersing them in DI water.

Intracellular Localization. The internalization and localization of $Co(OH)_2$ NS into the cells were evaluated by fluorescence probes. Typically, 150 000 cells were seeded into a transparent microplate containing a glass coverslip. To label $Co(OH)_2$ NS, 30 μg/mL rhodamine B was mixed with $Co(OH)_2$ NS under continuous rotation at room temperature for 1 h. Although this was passive loading, it may also induce the intercalation of small rhodamine B molecules inside the layer or cavities of layered double hydroxides isostructural $Co(OH)_2$ NS. Then, the cell lines were treated with 50 μg/mL $Co(OH)_2$ NS for different time points (1, 6, and 24 h). After washing with PBS two times, the cells were incubated according to the manufacturer's instructions with 200 nM LysoTracker Green DND-26 (Thermo Fisher Scientific) and 200 ng/mL Hoechst 33342 for lysosomes and nuclear staining, respectively. After that, the cells were fixed with paraformaldehyde 4% for 20 min and the coverslip was mounted using Fluorsave mounting media (Merck Millipore, Burlington, MA) for cellular imaging. Hoechst, LysoTracker Green DND-26, and Rhodamine B were detected under a fluorescence microscope with appropriate filters. Images were analyzed with ImageJ and JacoP plugins.

Flow Cytometry Analysis. Herein, 3×10^5 A2780 cells were grown as indicated by the supplier for indicated time points. Annexin V analysis was performed using PE-Annexin V Apoptosis Detection Kit from Becton−Dickinson (Franklin Lakes, NJ) according to the manufacturer's protocol using FACS Canto II from Becton−Dickinson (Franklin Lakes, NJ) and BD FACS DIVA software.

Cancer Organoids. Cancer organoids were obtained from totally anonymized specimens. However, biobank informed consent for research purposes was available to collect the samples at the National Cancer Institute (CRO) of Aviano, Italy. HGSOC specimens from ascites and tumor tissues were collected to generate organoids. Briefly, fluids were centrifuged (1000 rpm, 10 min) and cell pellets were washed in Hanks' Balanced Salt solution two times (HBSS, Gibco Cat. No. 14175-053). Cold red blood cell lysis buffer (Roche Diagnostics, Cat. No. 30020500) was added for lysis of erythrocytes. After 10 min on ice, the cells were centrifuged and resuspended in Cultrex growth factor-reduced Basement Membrane Extract (BME), Type2 (R&D Systems Cat. No. 3533-001-02). Differently, solid tumor tissue specimens were washed for 30 min in Dulbecco' s modified Eagle's medium/Nutrient Mixture F-12 Ham with antibiotics (Levofloxacin 100 μg/mL, Vancotex 25 μg/mL, Ciproxin 5 μg/mL, Gentamicin 200 μg/mL, Fungizone 5μg/mL). Then, the tissues were minced with fine scissors, treated with 2 mg/mL collagenase type I (Gibco Cat. No: 17018029) at 37 °C for 20 min. and mechanically dissociated by repetitive pipetting. After centrifugation, tissue fragments were resuspended in Cultrex growth factor-reduced BME, Type2. Both ascites and tissue organoids were seeded on a prewarmed 24-well cell culture plate, and after cultrex solidification, 450 μl of organoid medium derived from Kopper et al.[35] was added to each well. The medium was subsequently refreshed every 2−3 days.

Histopathology Analysis. Sections of formalin-fixed, paraffin-embedded ascites and solid tumor organoids were used for histopathological analyses. Organoids were collected, fixed in phosphate-buffered 10% formalin, and embedded in paraffin using Micro NextGen CelBloking Kit (Cat no: M20; AV BioInnovation) following manufacturer's instructions. Subsequently, 5 μm sections were stained with hematoxylin and eosin (H&E) using the Leica ST5020 multistainer and 2 μm sections were cut for IHC analysis. IHC staining was performed with UltraVision LP Detection System HRP DAB kit (Thermo Scientific, Waltham). Heat-induced antigen retrieval was performed using 10 mM citrate buffer pH 6.0. The following antibodies were used to characterize patient's derived organoids and parent tumor: PAX8 (ProteinTech Group, Germany, EU; 10336-1-AP); Ca125 (Santacruz Biotechnology, TX; sc-52095); WT1 (Abcam, U.K.; ab89901). Tissues were analyzed with a light microscope using different magnifications.

Statistical Analysis. Statistical analysis was performed using GraphPad Prism software, and a p value <0.05 was considered significant.

■ ASSOCIATED CONTENT

Supporting Information

The Supporting Information is available free of charge at https://pubs.acs.org/doi/10.1021/acsomega.1c03010.

UV−vis spectra, hematoxylin and eosin staining and IHC, and IC_{50} values distribution (PDF)

■ AUTHOR INFORMATION

Corresponding Author

Flavio Rizzolio − *Department of Molecular Sciences and Nanosystems, Ca'Foscari University of Venice, 30123 Venezia, Italy; Pathology Unit, Centro di Riferimento Oncologico di Aviano (CRO) IRCCS, 33081 Aviano, Italy;* orcid.org/0000-0002-3400-4363; Phone: (+39) 0412348910; Email: flavio.rizzolio@unive.it; Fax: (+39) 0434659370

https://doi.org/10.1021/acsomega.1c03010
ACS Omega 2021, 6, 28611−28619

Authors

Muhammad Adeel − *Department of Molecular Sciences and Nanosystems, Ca'Foscari University of Venice, 30123 Venezia, Italy; Pathology Unit, Centro di Riferimento Oncologico di Aviano (CRO) IRCCS, 33081 Aviano, Italy;* orcid.org/0000-0003-0916-4151

Salvatore Parisi − *Pathology Unit, Centro di Riferimento Oncologico di Aviano (CRO) IRCCS, 33081 Aviano, Italy*

Matteo Mauceri − *Department of Molecular Sciences and Nanosystems, Ca'Foscari University of Venice, 30123 Venezia, Italy*

Kanwal Asif − *Department of Molecular Sciences and Nanosystems, Ca'Foscari University of Venice, 30123 Venezia, Italy; Pathology Unit, Centro di Riferimento Oncologico di Aviano (CRO) IRCCS, 33081 Aviano, Italy*

Michele Bartoletti − *Department of Medicine (DAME), University of Udine, 33100 Udine, Italy; Unit of Medical Oncology and Cancer Prevention, Department of Medical Oncology, Centro di Riferimento Oncologico di Aviano (CRO), IRCCS, 33081 Aviano, Italy*

Fabio Puglisi − *Department of Medicine (DAME), University of Udine, 33100 Udine, Italy; Unit of Medical Oncology and Cancer Prevention, Department of Medical Oncology, Centro di Riferimento Oncologico di Aviano (CRO), IRCCS, 33081 Aviano, Italy*

Isabella Caligiuri − *Pathology Unit, Centro di Riferimento Oncologico di Aviano (CRO) IRCCS, 33081 Aviano, Italy*

Md. Mahbubur Rahman − *Department of Applied Chemistry, Konkuk University, 27478 Chungju, South Korea;* orcid.org/0000-0003-0012-5324

Vincenzo Canzonieri − *Pathology Unit, Centro di Riferimento Oncologico di Aviano (CRO) IRCCS, 33081 Aviano, Italy; Department of Medical, Surgical, and Health Sciences, University of Trieste, 34127 Trieste, Italy;* orcid.org/0000-0001-6010-0976

Complete contact information is available at: https://pubs.acs.org/10.1021/acsomega.1c03010

Notes

The authors declare no competing financial interest.

■ ACKNOWLEDGMENTS

This work was financially supported by AIRC (IG23566) and Italian Ministry of Health—Ricerca Corrente and POR FESR FVG 2014-2020: attività 1.3.b - CATHENA Project.

■ REFERENCES

(1) Vaughan, S.; Coward, J. I.; Bast, R. C.; Berchuck, A.; Berek, J. S.; Brenton, J. D.; Coukos, G.; Crum, C. C.; Drapkin, R.; Etemadmoghadam, D.; Friedlander, M.; Gabra, H.; Kaye, S. B.; Lord, C. J.; Lengyel, E.; Levine, D. A.; McNeish, I. A.; Menon, U.; Mills, G. B.; Nephew, K. P.; Oza, A. M.; Sood, A. K.; Stronach, E. A.; Walczak, H.; Bowtell, D. D.; Balkwill, F. R. Rethinking ovarian cancer: recommendations for improving outcomes. *Nat. Rev. Cancer* **2011**, *11*, 719−725.

(2) Havrilesky, L. J.; Lim, S.; Ehrisman, J. A.; Lorenzo, A.; Alvarez Secord, A.; Yang, J. C.; Johnson, F. R.; Gonzalez, J. M.; Reed, S. D. Patient preferences for maintenance PARP inhibitor therapy in ovarian cancer treatment. *Gynecol. Oncol.* **2020**, *156*, 561−567.

(3) Burger, R. A.; Brady, M. F.; Bookman, M. A.; Fleming, G. F.; Monk, B. J.; Huang, H.; Mannel, R. S.; Homesley, H. D.; Fowler, J.; Greer, B. E.; Boente, M.; Birrer, M. J.; Liang, S. X. Incorporation of bevacizumab in the primary treatment of ovarian cancer. *N. Engl. J. Med.* **2011**, *365*, 2473−2483.

(4) Russo Spena, C.; De Stefano, L.; Palazzolo, S.; Salis, B.; Granchi, C.; Minutolo, F.; Tuccinardi, T.; Fratamico, R.; Crotti, S.; D'Aronco, S.; Agostini, M.; Corona, G.; Caligiuri, I.; Canzonieri, V.; Rizzolio, F. Liposomal delivery of a Pin1 inhibitor complexed with cyclodextrins as new therapy for high-grade serous ovarian cancer. *J. Controlled Release* **2018**, *281*, 1−10.

(5) Ma, Z.; Xu, L.; Liu, D.; Zhang, X.; Di, S.; Li, W.; Zhang, J.; Reiter, R. J.; Han, J.; Li, X.; Yan, X. Utilizing Melatonin to Alleviate Side Effects of Chemotherapy: A Potentially Good Partner for Treating Cancer with Ageing. *Oxid. Med. Cell. Longevity* **2020**, *2020*, No. 6841581.

(6) Torricelli, P.; Antonelli, F.; Ferorelli, P.; Borromeo, I.; Shevchenko, A.; Lenzi, S.; De Martino, A. Oral nutritional supplement prevents weight loss and reduces side effects in patients in advanced lung cancer chemotherapy. *Amino Acids* **2020**, *52*, 445−451.

(7) Li, L. J.; Chong, Q.; Wang, L.; Cher, G. B.; Soo, R. A. Different treatment efficacies and side effects of cytotoxic chemotherapy. *J. Thorac. Dis.* **2020**, *12*, 3785−3795.

(8) Gupta, S.; Pathak, Y.; Gupta, M. K.; Vyas, S. P. Nanoscale drug delivery strategies for therapy of ovarian cancer: conventional vs targeted. *Artif. Cells, Nanomed., Biotechnol.* **2019**, *47*, 4066−4088.

(9) Bobo, D.; Robinson, K. J.; Islam, J.; Thurecht, K. J.; Corrie, S. R. Nanoparticle-Based Medicines: A Review of FDA-Approved Materials and Clinical Trials to Date. *Pharm. Res.* **2016**, *33*, 2373−2387.

(10) Bayda, S.; Hadla, M.; Palazzolo, S.; Riello, P.; Corona, G.; Toffoli, G.; Rizzolio, F. Inorganic Nanoparticles for Cancer Therapy: A Transition from Lab to Clinic. *Curr. Med. Chem.* **2017**, *25*, 4269−4303.

(11) Palazzolo, S.; Bayda, S.; Hadla, M.; Caligiuri, I.; Corona, G.; Toffoli, G.; Rizzolio, F. The Clinical Translation of Organic Nanomaterials for Cancer Therapy: A Focus on Polymeric Nanoparticles, Micelles, Liposomes and Exosomes. *Curr. Med. Chem.* **2018**, *25*, 4224−4268.

(12) Mohd-Zahid, M. H.; Mohamud, R.; Che Abdullah, C. A.; Lim, J.; Alem, H.; Wan Hanaffi, W. N.; Iskandar, Z. A. Colorectal cancer stem cells: A review of targeted drug delivery by gold nanoparticles. *RSC Adv.* **2020**, *10*, 973−985.

(13) Lepeltier, E.; Rijo, P.; Rizzolio, F.; Popovtzer, R.; Petrikaite, V.; Assaraf, Y. G.; Passirani, C. Nanomedicine to target multidrug resistant tumors. *Drug Resist. Updates* **2020**, *52*, No. 100704.

(14) Rizzolio, F. Nanomedicine in Cancer Pathology. *Curr. Med. Chem.* **2018**, *25*, 4190−4191.

(15) Raza, A.; Sime, F. B.; Cabot, P. J.; Maqbool, F.; Roberts, J. A.; Falconer, J. R. Solid nanoparticles for oral antimicrobial drug delivery: a review. *Drug Discovery Today* **2019**, *24*, 858−866.

(16) Jahangirian, H.; Kalantari, K.; Izadiyan, Z.; Rafiee-Moghaddam, R.; Shameli, K.; Webster, T. J. A review of small molecules and drug delivery applications using gold and iron nanoparticles. *Int. J. Nanomed.* **2019**, *14*, 1633−1657.

(17) Narvekar, M.; Xue, H. Y.; Eoh, J. Y.; Wong, H. L. Nanocarrier for poorly water-soluble anticancer drugs - Barriers of translation and solutions. *AAPS PharmSciTech* **2014**, *15*, 822−833.

(18) Acosta, E. Bioavailability of nanoparticles in nutrient and nutraceutical delivery. *Curr. Opin. Colloid Interface Sci.* **2009**, *14*, 3−15.

(19) Zaman, Z. Addressing Solubility through Nano Based Drug Delivery Systems. *J. Nanomed. Nanotechnol.* **2016**, *7*, 1−7.

(20) Park, J.; Choi, Y.; Chang, H.; Um, W.; Ryu, J. H.; Kwon, I. C. Alliance with EPR effect: Combined strategies to improve the EPR effect in the tumor microenvironment. *Theranostics* **2019**, *9*, 8073−8090.

(21) Patra, J. K.; Das, G.; Fraceto, L. F.; Campos, E. V. R.; Rodriguez-Torres, M. D. P.; Acosta-Torres, L. S.; Diaz-Torres, L. A.; Grillo, R.; Swamy, M. K.; Sharma, S.; Habtemariam, S.; Shin, H. S. Nano based drug delivery systems: Recent developments and future prospects. *J. Nanobiotechnol.* **2018**, *16*, No. 71.

(22) Chenthamara, D.; Subramaniam, S.; Ramakrishnan, S. G.; Krishnaswamy, S.; Essa, M. M.; Lin, F. H.; Qoronfleh, M. W.

Therapeutic efficacy of nanoparticles and routes of administration. *Biomater. Res.* **2019**, *23*, 1−29.
(23) Kumar, V.; Palazzolo, S.; Bayda, S.; Corona, G.; Toffoli, G.; Rizzolio, F. DNA nanotechnology for cancer therapy. *Theranostics* **2016**, *6*, 710−725.
(24) Adeel, M.; Duzagac, F.; Canzonieri, V.; Rizzolio, F. Self-Therapeutic Nanomaterials for Cancer Therapy: A Review. *ACS Appl. Nano Mater.* **2020**, *3*, 4962−4971.
(25) Wilhelm, S.; Tavares, A. J.; Dai, Q.; Ohta, S.; Audet, J.; Dvorak, H. F.; Chan, W. C. W. Analysis of nanoparticle delivery to tumours. *Nat. Rev. Mater.* **2016**, *1*, No. 16014.
(26) Kowalski, P. S.; Bhattacharya, C.; Afewerki, S.; Langer, R. Smart Biomaterials: Recent Advances and Future Directions. *ACS Biomater. Sci. Eng.* **2018**, *4*, 3809−3817.
(27) Jaishankar, M.; Tseten, T.; Anbalagan, N.; Mathew, B. B.; Beeregowda, K. N. Toxicity, mechanism and health effects of some heavy metals. *Interdiscip. Toxicol.* **2014**, *7*, 60−72.
(28) Gardner, F. H. The use of cobaltous chloride in the anemia associated with chronic renal disease. *J. Lab Clin. Med.* **1953**, *41*, 56−64.
(29) Munteanu, C. R.; Suntharalingam, K. Advances in cobalt complexes as anticancer agents. *Dalton Trans.* **2015**, *44*, 13796−13808.
(30) Thamilarasan, V.; Sengottuvelan, N.; Sudha, A.; Srinivasan, P.; Chakkaravarthi, G. Cobalt(III) complexes as potential anticancer agents: Physicochemical, structural, cytotoxic activity and DNA/protein interactions. *J. Photochem. Photobiol., B* **2016**, *162*, 558−569.
(31) Klein, S.; Kızaloğlu, M.; Portilla, L.; Park, H.; Rejek, T.; Hümmer, J.; Meyer, K.; Hock, R.; Distel, L. V. R.; Halik, M.; Kryschi, C. Enhanced In Vitro Biocompatibility and Water Dispersibility of Magnetite and Cobalt Ferrite Nanoparticles Employed as ROS Formation Enhancer in Radiation Cancer Therapy. *Small.* **2018**, *14*, No. 1704111.
(32) Bejarbaneh, M.; Moradi-Shoeili, Z.; Jalali, A.; Salehzadeh, A. Synthesis of Cobalt Hydroxide Nano-flakes Functionalized with Glutamic Acid and Conjugated with Thiosemicarbazide for Anticancer Activities Against Human Breast Cancer Cells. *Biol. Trace Elem. Res.* **2020**, *198*, 98−108.
(33) Law, B. Y. K.; Qu, Y. Q.; Mok, S. W. F.; Liu, H.; Zeng, W.; Han, Y.; Gordillo-Martinez, F.; Chan, W. K.; Wong, K. M. C.; Wong, V. K. W. New perspectives of cobalt tris(bipyridine) system: Anti-cancer effect and its collateral sensitivity towards multidrug-resistant (MDR) cancers. *Oncotarget* **2017**, *8*, 55003−55021.
(34) Heffern, M. C.; Yamamoto, N.; Holbrook, R. J.; Eckermann, A. L.; Meade, T. J. Cobalt derivatives as promising therapeutic agents. *Curr. Opin. Chem. Biol.* **2013**, *17*, 189−196.
(35) Kopper, O.; de Witte, C. J.; Lõhmussaar, K.; Valle-Inclan, J. E.; Hami, N.; Kester, L.; Balgobind, A. V.; Korving, J.; Proost, N.; Begthel, H.; van Wijk, L. M.; Revilla, S. A.; Theeuwsen, R.; van de Ven, M.; van Roosmalen, M. J.; Ponsioen, B.; Ho, V. W. H.; Neel, B. G.; Bosse, T.; Gaarenstroom, K. N.; Vrieling, H.; Vreeswijk, M. P. G.; van Diest, P. J.; Witteveen, P. O.; Jonges, T.; Bos, J. L.; van Oudenaarden, A.; Zweemer, R. P.; Snippert, H. J. G.; Kloosterman, W. P.; Clevers, H. An organoid platform for ovarian cancer captures intra- and interpatient heterogeneity. *Nat. Med.* **2019**, *25*, 838−849.
(36) Tricoli, V.; Orsini, G.; Anselmi, M. Ion transport in a class of imidazole-based liquid/solid protic ionics. *Phys. Chem. Chem. Phys.* **2012**, *14*, 10979−10986.
(37) Su, D.; Xie, X.; Munroe, P.; Dou, S.; Wang, G. Mesoporous hexagonal Co3O4 for high performance lithium ion batteries. *Sci. Rep.* **2014**, *4*, No. 6519.
(38) Shackery, I.; Patil, U.; Pezeshki, A.; Shinde, N. M.; Kang, S.; Im, S.; Jun, S. C. Copper Hydroxide Nanorods Decorated Porous Graphene Foam Electrodes for Non-enzymatic Glucose Sensing. *Electrochim. Acta* **2016**, *191*, 954−961.
(39) Li, R.; Hu, Z.; Shao, X.; Cheng, P.; Li, S.; Yu, W.; Lin, W.; Yuan, D. Large scale synthesis of NiCo layered double hydroxides for superior asymmetric electrochemical capacitor. *Sci. Rep.* **2016**, *6*, No. 3572.
(40) Kim, M.; Nam, D. H.; Park, H. Y.; Kwon, C.; Eom, K.; Yoo, S.; Jang, J.; Kim, H. J.; Cho, E.; Kwon, H. Cobalt-carbon nanofibers as an efficient support-free catalyst for oxygen reduction reaction with a systematic study of active site formation. *J. Mater. Chem. A* **2015**, *3*, 14284−14290.
(41) Paustenbach, D. J.; Tvermoes, B. E.; Unice, K. M.; Finley, B. L.; Kerger, B. D. A review of the health hazards posed by cobalt. *Crit. Rev. Toxicol.* **2013**, *43*, 316−362.
(42) Hraběta, J.; Belhajová, M.; Šubrtová, H.; Rodrigo, M. A. M.; Heger, Z.; Eckschlager, T. Drug sequestration in lysosomes as one of the mechanisms of chemoresistance of cancer cells and the possibilities of its inhibition. *Int. J. Mol. Sci.* **2020**, *21*, No. 4392.
(43) Kipps, E.; Tan, D. S. P.; Kaye, S. B. Meeting the challenge of ascites in ovarian cancer: New avenues for therapy and research. *Nat. Rev. Cancer* **2013**, *13*, 273−282.
(44) Smolle, E.; Taucher, V.; Haybaeck, J. Malignant ascites in ovarian cancer and the role of targeted therapeutics. *Anticancer Res.* **2014**, *34*, 1553−1562.
(45) Palazzolo, S.; Hadla, M.; Spena, C. R.; Caligiuri, I.; Rotondo, R.; Adeel, M.; Kumar, V.; Corona, G.; Canzonieri, V.; Toffoli, G.; Rizzolio, F. An effective multi-stage liposomal DNA origami nanosystem for in vivo cancer therapy. *Cancers* **2019**, *11*, No. 1997.
(46) Granchi, C.; Bononi, G.; Ferrisi, R.; Gori, E.; Mantini, G.; Glasmacher, S.; Poli, G.; Palazzolo, S.; Caligiuri, I.; Rizzolio, F.; Canzonieri, V.; Perin, T.; Gertsch, J.; Sodi, A.; Giovannetti, E.; Macchia, M.; Minutolo, F.; Tuccinardi, T.; Chicca, A. Design, synthesis and biological evaluation of second-generation benzoylpiperidine derivatives as reversible monoacylglycerol lipase (MAGL) inhibitors. *Eur. J. Med. Chem.* **2021**, *209*, No. 112857.
(47) Scattolin, T.; Bortolamiol, E.; Visentin, F.; Palazzolo, S.; Caligiuri, I.; Perin, T.; Canzonieri, V.; Demitri, N.; Rizzolio, F.; Togni, A. Palladium(II)-η3-Allyl Complexes Bearing N-Trifluoromethyl N-Heterocyclic Carbenes: A New Generation of Anticancer Agents that Restrain the Growth of High-Grade Serous Ovarian Cancer Tumoroids. *Chem. - Eur. J.* **2020**, *26*, 11868−11876.
(48) Duzagac, F.; Saorin, G.; Memeo, L.; Canzonieri, V.; Rizzolio, F. Microfluidic organoids-on-a-chip: Quantum leap in cancer research. *Cancers* **2021**, *13*, 1−35.
(49) Hill, S. J.; Decker, B.; Roberts, E. A.; Horowitz, N. S.; Muto, M. G.; Worley, M. J.; Feltmate, C. M.; Nucci, M. R.; Swisher, E. M.; Nguyen, H.; Yang, C.; Morizane, R.; Kochupurakkal, B. S.; Do, K. T.; Konstantinopoulos, P. A.; Liu, J. F.; Bonventre, J. V.; Matulonis, U. A.; Shapiro, G. I.; Berkowitz, R. S.; Crum, C. P.; D'Andrea, A. D. Prediction of DNA Repair Inhibitor Response in Short Term Patient-Derived Ovarian Cancer Organoids. *Cancer Discovery* **2018**, *8*, 1404−1421.
(50) Yamada, K. Cobalt: Its role in health and disease. *Met. Ions Life Sci.* **2013**, *13*, 295−320.
(51) Leyssens, L.; Vinck, B.; Van Der Straeten, C.; Wuyts, F.; Maes, L. Cobalt toxicity in humans—A review of the potential sources and systemic health effects. *Toxicology* **2017**, *387*, 43−56.
(52) Rohn, R. J.; Bond, W. H.; Klotz, L. J. The effect of cobalt-iron therapy in iron deficiency anemia in infants. *J. Indiana State Med. Assoc.* **1953**, *46*, 1253−1260.
(53) Rohn, R. J.; Bond, W. H. Observations on some hematological effects of cobalt-iron mixtures. *Lancet* **1953**, *73*, 317−324.

https://doi.org/10.1021/acsomega.1c03010
ACS Omega 2021, 6, 28611−28619